Ocean Modelling 174 (2022) 102030

Contents lists available at ScienceDirect

Ocean Modelling

journal homepage: www.elsevier.com/locate/ocemod

An empirical method for predicting the South China Sea Warm Current from wind stress using Ekman dynamics

Zhitao Yu *, Yalin Fan, E. Joseph Metzger

Naval Research Laboratory, Stennis Space Center, MS, USA

ARTICLE INFO

Keywords:
South China Sea Warm Current
Ekman dynamics
Continental shelf
Wind stress
Empirical orthogonal function
HYCOM reanalysis

ABSTRACT

An empirical method is developed to predict the counter-wind South China Sea Warm Current (SCSWC) using wind stress at a specific location that is built on the most dominant Empirical Orthogonal Function (EOF) mode of the Sea Surface Height (SSH), i.e. the Ekman mode (Yu et al., 2021). Based on the most dominant EOF modes from a 22-year HYbrid Coordinate Ocean Model (HYCOM) reanalysis, a rectangular box and a specific location are carefully chosen for SSH and wind stress, respectively. In the rectangular box (specific location), more than 90% of the SSH (wind stress) variance is explained by the most dominant EOF mode. SSH in the rectangular box is predicted from the wind stress at the specific location. When the average cross-shore pressure gradient force in the rectangular box is negative, the SCSWC exists in the model solution. The critical alongshore (38° to the north of east) wind stress at the specific location is −0.117 N/m^2. The SCSWC occurs in the rectangular box when the wind further relaxes. The accuracy of this method varies from 74.9% to 75.3% and the representativeness varies from 84.5% to 85.9% with time lags from 12 to 16 h when applying the method to predict the SCSWC during the 21-winters in HYCOM reanalysis.

1. Introduction

The South China Sea (SCS) is the largest marginal sea in Southeast Asia and its continental shelf is one of the widest in the world ocean (Guan and Fang, 2006) as shown in Fig. 1. The seasonally reversing East Asia monsoon wind plays a prominent role in forcing the seasonally varying circulation in the SCS (Wyrtki, 1961; Shaw and Chao, 1994). Northeasterly winds prevail over the region in winter and thus, it was thought that the currents over the continental shelf in the northern SCS flow from northeast towards the southwest following the wind (Wyrtki, 1961).

The northeastward counter-wind South China Sea Warm Current (SCSWC) was first discovered in winter by Guan and Chen (1964) using hydrographic data obtained during the Chinese National Comprehensive Oceanographic Survey during 1958 to 1960 (Hu et al., 2000). Since then, the existence of the SCSWC has been confirmed by repeated observations (Guan, 1986; Guan and Fang, 2006), and it was commonly described as a narrow and strong northeastward current persisting all winter long (Su and Wang, 1987; Hu et al., 2000) and originating from Hainan Island (Li et al., 1992; Hu et al., 2000; Guan and Fang, 2006; Yang et al., 2008).

The SCSWC has been drawn much attention from the scientific community due to its nonintuitive counter-wind property in winter seasons after its first observation 60 years ago. The main proposed generation mechanism is Kuroshio intrusion into the SCS via Luzon Strait (Su and Wang, 1987; Zhong, 1990; Li et al., 1993; Ye, 1994; Xue et al., 2004) to elevate the Sea Surface Height (SSH) near the shelf break. Another proposed generation mechanism is related to the alongshore SSH slope (Zeng et al., 1989; Li et al., 1992; Hsueh and Zhong, 2004), higher near Hainan Island and lower at Taiwan Strait. Besides the two main proposed mechanisms, the following provide different points of view on the formation of the SCSWC. Zhai et al. (2004) proposed that the anticyclonic wind stress curl in the northernmost SCS could generate the SCSWC in winter. The importance of Taiwan Strait was illustrated through numerical simulations by Yang et al. (2008) who demonstrated that the SCSWC vanishes when the Taiwan Strait is closed. Wang et al. (2010) suggested the Joint Effect of Baroclinicity and Relief drives the SCSWC against the wind in winter.

From the wide variety of explanations, it is fair to say that there still is no agreed upon consensus within the scientific community for the dynamics that controls the SCSWC. Chao et al. (1995) were the first to suggest wind relaxation as a possible generation mechanism when the alongshore SSH slope exists. Their hypothesis was supported by Chiang et al. (2008). The appearance of the SCSWC in winter is well documented when winds relax but lacked a plausible explanation (Guan and Fang, 2006). Yu et al. (2021) performed an Extended Empirical Orthogonal Function (EEOF) analysis of the hourly SSH and wind stress anomalies from a 22-year global HYbrid Coordinate Ocean Model (HYCOM) data-assimilative reanalysis. They also suggest that wind

* Correspondence to: Ocean Sciences Division, Naval Research Laboratory, Stennis Space Center, MS 39529, USA
E-mail address: zhitao.yu@nrlssc.navy.mil (Z. Yu).

https://doi.org/10.1016/j.ocemod.2022.102030
Received 26 January 2022; Received in revised form 20 April 2022; Accepted 19 May 2022
Available online 25 May 2022
1463-5003/Published by Elsevier Ltd.

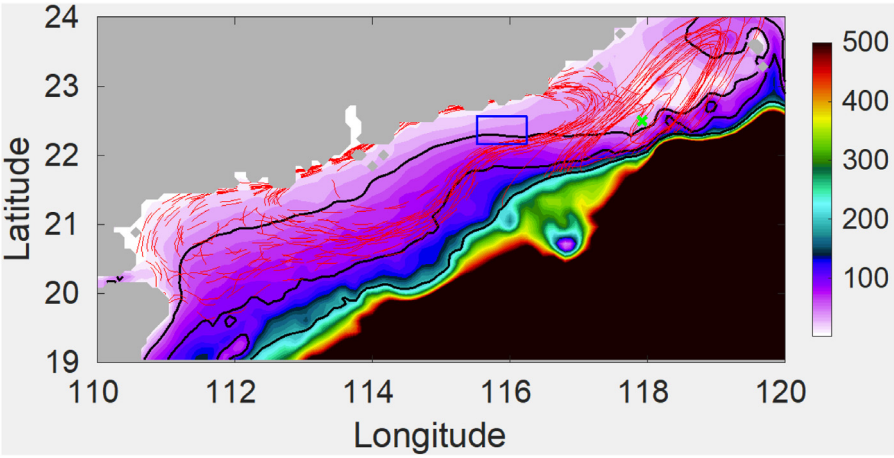

Fig. 1. HYCOM bathymetry (meters) for the South China Sea. The land–ocean boundary is defined by the 10 cm isobaths but all depths less than 5 m are set to 5 m. The three black solid lines indicate the 50, 100, and 200 m isobaths, respectively. The blue box defines the region of the South China Sea Warm Current detection. The green X near 118°E, 22.5°N represents the location at which the alongshore wind stress is used to predict the South China Sea Warm Current in the blue box. Red dashed (solid) lines represent the contour lines of the 90% local SSH (alongshore wind stress) variance explained by the dominant mode.

relaxation is the primary driving mechanism of the SCSWC but with an entirely different dynamical explanation than Chiang et al. (2008). There are two pathways, direct and indirect, via which the SCSWC is driven by the wind relaxation. The direct pathway, in the alongshore direction, is that wind stress represents a weaker force when winds relax. The indirect pathway is the offshore Ekman transport anomaly associated with wind relaxation. Yu et al. (2021) reveal that (1) the wind relaxation reverses the mean offshore pressure gradient force (Fig. 2a, solid green arrow) to a favorable onshore pressure gradient force (Fig. 2b, solid green arrow) over the continental shelf via offshore Ekman transport anomaly, and (2) the sum of the northeastward alongshore pressure gradient force and the southeastward alongshore kinematic wind stress is northeastward (Fig. 2b, dashed green arrow) due to the dominance of the former over the latter when wind relaxes. Thus, there is a need to have counter-wind currents (Fig. 2b, dashed gray arrow) in winter when the wind relaxes so that the bottom friction, opposite to the current direction, joins the relaxed northeasterly wind stress to balance the northeastward alongshore pressure gradient force. The SCSWC is positioned between the southwestward Guangdong coastal current (Fig. 2b, thin black arrow) and the southwestward South China Sea Branch of Kuroshio (Fig. 2b, heavy black arrow). The opposite is true with the mean and strong monsoon wind scenario as currents move southwestward over the whole shelf (Fig. 2a). Wind relaxation as the generation mechanism of the SCSWC implies that it cannot be persistent but rather is intermittent. This agrees well with Fang et al. (2015) since they did not observe the persistent counter-wind SCSWC over the continental shelf in the northern SCS in 2006 and 2007. Yu et al. (2021) also conclude that the SCSWC originates in the area south of Taiwan Strait due to the dynamics mentioned above, contrary to the commonly accepted origination near Hainan Island.

The wind relaxation mechanism proposed by Yu et al. (2021) suggests the two dominant parameters that control the generation of the SCSWC are SSH and wind stress. Thus, it is possible to predict the appearance of the SCSWC using these two variables through either the cross-shore dynamics threshold when the cross-shore pressure gradient force is negative (solid green arrow in Fig. 2b, $-g\frac{\partial SSH}{\partial x} < 0$, where g is gravitational parameter) or the alongshore dynamics when the sum of alongshore pressure gradient force and alongshore wind stress is positive (dashed green arrow in Fig. 2b, $-g\frac{\partial SSH}{\partial y} + \frac{\tau}{\rho_o H} > 0$, where τ is alongshore wind stress, ρ_o is a reference density for seawater, and H is the water depth). The goal of this research is to use the wind stress at a specific location to predict SSH which will lead to the SCSWC prediction based on either the cross-shore or alongshore dynamics threshold.

In this work, we present an empirical method to predict the SCSWC from wind stress based on the dynamics revealed by Yu et al. (2021). The method predicts SSH in a rectangular box (0.8° x 0.5°) over the northern continental shelf of the SCS (Fig. 1, blue box) at time t from the alongshore wind stress at t minus *LAG* (t-*LAG*), where *LAG* varies and is defined in Section 3, at a specific location (118°E, 22.5°N). How to choose the rectangular box for SSH and the specific location for wind stress will be introduced in Section 3.3. The predicted SSH is then used to calculate the two thresholds mentioned above to predict the existence of the SCSWC. The method is easy to use and has high accuracy to predict the SCSWC. This paper is organized as follows: Section 2 introduces the numerical model and data sets used for this research. Section 3 describes the empirical method developed from the Ekman dynamics. Results are shown in Section 4, which is followed by the conclusions and discussions in Section 5.

2. Numerical model and data

A 22-year global HYCOM reanalysis from 1994 to 2015 (https://www.hycom.org/dataserver/gofs-3pt1/reanalysis) and four winter seasons (December 2017 to February, 2021) of daily operational Global Ocean Forecast System (GOFS) 3.1 7.5-day forecasts are used in this study. The HYCOM reanalysis is used to calculate the empirical regression coefficient of mode 1 SSH Empirical Orthogonal Function (EOF) against the mode 1 alongshore wind stress EOF in the 21 winter seasons in the rectangular box (Fig. 1). Both data sets are used to test the accuracy of the prediction method developed in Section 3.

HYCOM is the ocean model component for the present operational US Navy GOFS 3.1 (Metzger et al., 2014). HYCOM is widely used in the ocean community (https://www.hycom.org) and a detailed description of its physics is provided by Bleck (2002). We briefly describe the model setup below with emphasis on the numerical aspects that are most relevant to this study. There are no tides or surface waves in both the HYCOM reanalysis and operational GOFS 3.1.

2.1. Model grids and output

The global HYCOM horizontal resolution for both the reanalysis and GOFS 3.1 is 0.08° (1/12.5°) that is ~9 km at the equator and ~8.2 km in the northern SCS. The grid is uniform cylindrical from 78.64°S–66°S, Mercator between 66°S–47°N and includes a bipolar patch north

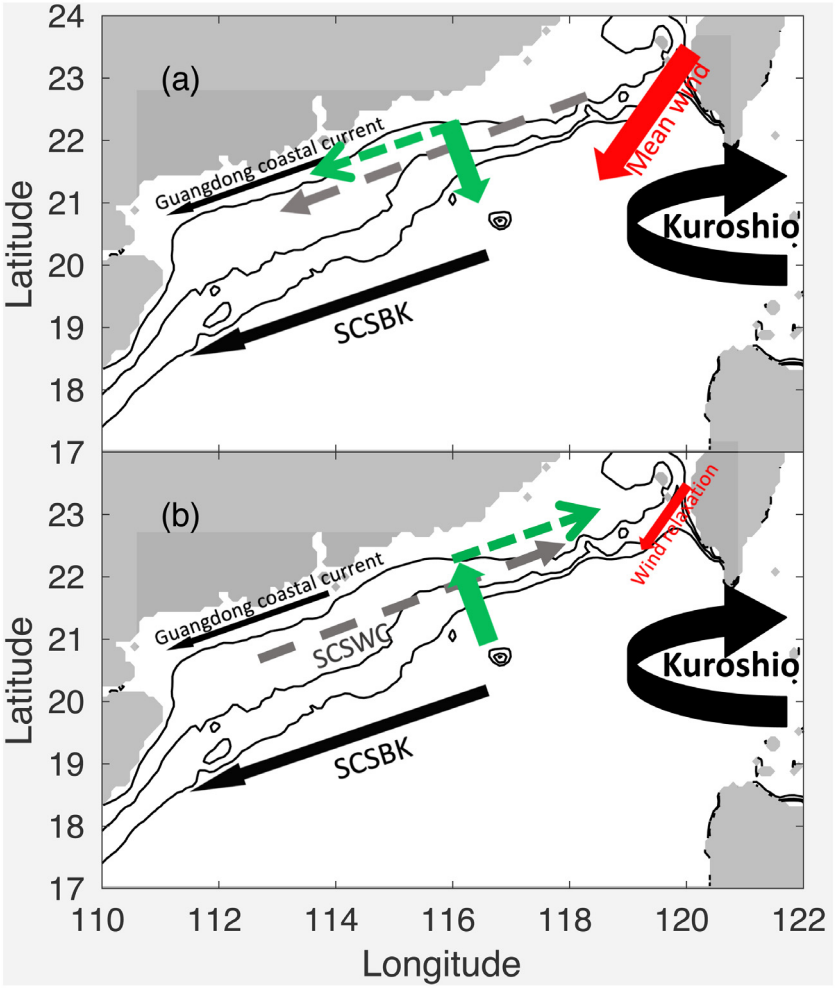

Fig. 2. Schematics showing currents over the continental shelf under (a) mean or strong northeasterly Monsoon wind and (b) wind relaxation. Red arrows represent the wind, curved black arrows represent the Kuroshio, thin black arrows near the coast represent the Guangdong coastal current, heavy black arrows over the shelf break represent the South China Sea Branch of Kuroshio, solid green arrows represent the cross-shore pressure gradient force, the dashed green arrows represent the sum of the alongshore pressure gradient force and the alongshore wind stress, and the dashed gray arrow in (b) represents the South China Sea Warm Current (SCSWC). The three black solid lines indicate the 50, 100, and 200 m isobaths, respectively.

of 47°N providing ~3.5 km grid spacing at the North Pole. Three coordinates coexist in HYCOM vertically: z-coordinates in unstratified water, sigma-coordinates in shallow depths, and isopycnal coordinates in the stratified ocean. There are 41 hybrid coordinate layers vertically with potential density referenced to 2000 m. The top 14 layers are always sigma-z so that water shallower than 84 m is always in fixed coordinates. For this study, we use wind stress, SSH, and barotropic velocity output. Hourly instantaneous wind stress, SSH, and barotropic velocity fields are interpolated to a uniform 0.08° resolution.

2.2. Data assimilation

Both the HYCOM reanalysis and operational GOFS 3.1 use the Navy Coupled Ocean Data Assimilation (NCODA) methodology (Cummings and Smedstad, 2014) to assimilate remotely sea surface temperature, SSH, sea ice concentration, and in-situ observations of temperature and salinity. An NCODA analysis relative to the 24-hour model forecast is valid at 12Z. HYCOM runs forward each day starting at 09Z with the incremental analysis update (Bloom et al., 1996) window between 09Z → 12Z, i.e. starting before the NCODA analysis time. At 12Z, HYCOM has fully assimilated all the observational data and the nowcast time (tau 000) and NCODA analysis time are synchronized. The reanalysis then runs in forecast mode only long enough to get to the next cycle point (36 h) whereas operational GOFS 3.1 runs in forecast mode out to 7.5 days.

2.3. Surface forcing

The wind stress formulation in both the HYCOM reanalysis and operational GOFS 3.1 forecasts includes the ocean surface currents (Yu et al., 2017). The wind stress is calculated at every time step taking into account the ocean surface currents as shown below

$$\boldsymbol{\tau} = \rho_{air} C_d \left|\boldsymbol{V}_{\mathbf{10}} - \boldsymbol{V}_o\right| (\boldsymbol{V}_{\mathbf{10}} - \boldsymbol{V}_o), \tag{1}$$

where, ρ_{air} is the air density at sea level, C_d is the drag coefficient, and $\boldsymbol{V}_{\mathbf{10}}$ is the 10-m wind velocity, and $\boldsymbol{V}_o$ is the velocity of ocean surface currents at 1 m depth. Bold fonts in (1) represent vectors. $\boldsymbol{V}_{\mathbf{10}}$ in the HYCOM reanalysis comes from the 0.3125° hourly National Centers for Environmental Prediction (NCEP) Climate Forecast System Reanalysis (CFSR) (Saha et al., 2010) before 2011 and the Climate Forecast System Version 2 (CFSV2) (Saha et al., 2014) from 2011 to 2015. Operational GOFS 3.1 uses 3-hourly $\boldsymbol{V}_{\mathbf{10}}$ from the 0.28125° NAVy Global Environmental Model (NAVGEM) (Hogan et al., 2014). HYCOM interpolates the CFSR, CFSV2, and NAVGEM from their native grids to the HYCOM grid and linearly interpolates the hourly and 3-hourly $\boldsymbol{V}_{\mathbf{10}}$ at each time step.

3. Method

In this section, we develop an empirical method to predict the SCSWC based on the linear dynamics revealed by Yu et al. (2021).

The authors demonstrated that the most dominant SSH mode in the northern SCS continental shelf is an Ekman mode through an EEOF analysis of the hourly SSH and wind stress data over 21 winter seasons from the HYCOM reanalysis. In the cross-shore direction, it is mainly governed by geostrophy. When alongshore wind stress is less than the alongshore pressure gradient force due to wind relaxation, friction generated by the counter wind SCSWC is required to balance the alongshore pressure gradient force with the alongshore wind stress.

The empirical method is developed based on the Ekman mode, the most dominant SSH mode. Since the Ekman mode is not a propagating mode, an EOF analysis is used instead of an EEOF for simplicity. Because the SSH over the open ocean is mainly driven by wind stress curl, the Ekman mode is only important over the continental shelf (Fig. 7, Yu et al., 2021). Thus, our analysis will only be performed over the shelf with the SSH and wind stress masked out in deep water where the bathymetry is more than 200 m.

3.1. Empirical orthogonal function of the reanalysis

Results from December 1994 to February 1995 (Fig. 3) are shown as an example to be consistent with Yu et al. (2021) and the coordinates are chosen so that the y-axis (alongshore) runs approximately parallel to the coast, positive towards the northeast and the positive x-axis points offshore. The orientation of the y-axis is estimated to be 38° to the north of east. The most dominant mode indicates that lower SSH anomaly (Fig. 3a) is generated by the positive alongshore wind stress anomaly (Fig. 3c), which is wind relaxation since the mean wind stress is southwestward (Yu et al., 2021). Their principle component time series are highly correlated with a correlation coefficient of 0.94 and significant to the 99% confidence level (Fig. 3b). The time lag *LAG*, as mentioned first in Section 1, associated with this correlation is 14 h with the variation of alongshore wind stress leading the SSH variation.

In the 1995 winter season (December 1994 to February 1995), the most dominant mode explains 85% and 74% of the total variance of the SSH and alongshore wind stress, respectively. In the 21 winter seasons, the total variance explained by the dominant mode varies from 79% to 87% (Fig. 4, solid line) for the SSH and 62% to 81% for the alongshore wind stress (Fig. 4, dashed line). The most dominant mode explains more SSH variations than alongshore wind stress in each of the 21 winter seasons.

In each of the 21 winter seasons, the principle component time series of the dominant mode for the SSH and alongshore wind stress are correlated, significant to the 99% confidence level as in 1995. The highest correlation coefficient varies from 0.83 to 0.94 (Fig. 5a, solid line) during the 21 winter seasons. The time lag, *LAG*, associated with these highest correlations varies from 12 to 16-hours (Fig. 5b). Applying these time lags to the corresponding principle component time series of the dominant mode, we can calculate the linear regression coefficient (*LRC*) between them since they are highly correlated. The *LRC* of the mode 1 SSH principle component time series against the mode 1 alongshore wind stress principle component time series varies from 0.71 to 0.90 (Fig. 5a, dashed line) during the first 21 winter seasons, and is 0.88 in 1995. The intercepts are negligible. This suggests that at any time instance t, we can estimate the principle component time series of the dominant SSH mode, $SSH\_ts1(t)$, as

$$SSH\_ts1(t) = LRC \times \tau\_ts1(t - LAG), \tag{2}$$

where, τ_ts1 is the mode 1 alongshore wind stress principle component time series.

3.2. Empirical method

We can use the EOFs to reconstruct the most dominant mode of the SSH and alongshore wind stress anomalies at time instance t and location (i, j) using the SSH and wind stress principle component time series as given in Eq. (2) as

$$SSHa1\,(i,j,t) = SSH\_EOF1(i,j) \times SSH\_ts1(t), \tag{3}$$

and

$$\tau a1(i,j,t) = \tau\_EOF1(i,j) \times \tau\_ts1(t), \tag{4}$$

where, $SSHa1$ is the SSH anomaly reconstructed from the most dominant SSH mode, SSH_EOF1, and $\tau a1$ is the alongshore wind stress anomaly reconstructed from the mode dominant alongshore wind stress mode, τ_EOF1. Divide Eq. (3) by (4) and rearrange to give

$$SSHa1\,(i,j,t) = \frac{SSH\_EOF1(i,j)}{\tau\_EOF1(i,j)} \times \frac{SSH\_ts1(t)}{\tau\_ts1(t)} \times \tau a1\,(i,j,t)\,. \tag{5}$$

For wind stress at a specific location $(i\tau, j\tau)$ and time instance $t - LAG$, after substitution of Eq. (2), Eq. (5) becomes

$$SSHa1\,(i,j,t) = \frac{SSH\_EOF1(i,j)}{\tau\_EOF1(i\tau,j\tau)} \times LRC \times \tau a1\,(i\tau,j\tau,t - LAG)\,. \tag{6}$$

If we define a regression coefficient of the mode 1 SSH EOF anomaly against the mode 1 alongshore wind stress anomaly, $RC(i,j)$, as

$$RC(i,j) = \frac{SSH\_EOF1(i,j)}{\tau\_EOF1(i\tau,j\tau)} \times LRC. \tag{7}$$

then, we can predict $SSHa1(i,j,t)$ from $\tau a1\,(i\tau, j\tau, t - LAG)$ once $RC(i,j)$ is given. However, when we only have a time series of wind stress forecasts, we do not have enough information to calculate the mode 1 alongshore wind stress anomaly, $\tau a1$. Details on how to solve this problem are given in Section 3.5. Furthermore, for the predicted mode 1 SSH anomaly, we do not have other SSH modes to reconstruct a reliable SSH field. To solve this, we need to define an area where the SSH (alongshore wind stress) anomaly is dominated by the corresponding mode 1 anomaly. And thus, we can use alongshore wind stress at a specific location to predict SSH in the chosen area.

3.3. How to choose the area for SSH predictions

Fig. 4 demonstrates that the most dominant mode explains more than 79% (62%) of the total SSH (alongshore wind stress) variance in all the 21 winter seasons. But this does not mean that the local variance explained by the most dominant mode is the same as the total variance explained. At some locations, the local variance explained by the most dominant mode can be much higher or lower than the total variance explained by the same mode. In this section, we calculate maps of the local variance explained by the most dominant mode. In the area where more than 90% of the local variance is explained by the most dominant mode, we assume the anomaly in the area is purely the mode 1 anomaly (i.e., $SSHa = SSHa1$).

To calculate the map of the local variance explained by the most dominant mode, we first calculate the most dominant mode homogeneous correlation map, which is defined as a map of the correlation coefficient between the most dominant mode principal component time series (Fig. 3b) of SSH (alongshore wind stress) and their corresponding original time series at each grid point. This is a useful indicator of the spatial localization of the co-varying part between the data and its most dominant mode, and the square of this variable represents the local variance explained by the most dominant mode. The red dashed (solid) lines in Fig. 1 represent the contours of the 90% local SSH (alongshore wind stress) variance explained by the dominant mode during the 21 winter seasons. For SSH, the Ekman mode explains more than 90% of the local variation in most of the areas shallower than 100 m to the south of 23°N. For the alongshore wind stress, the area is much smaller and mainly located at the northeastern continental shelf to the southwest of Taiwan Strait (Fig. 1). Please note that the maximum local alongshore wind stress variance explained by the most dominant mode in 2005 is 88.9%, slightly less than 90% criterion.

The specific location for wind stress should be located within the common border of all the 90% local variance contours. There are 4 grid

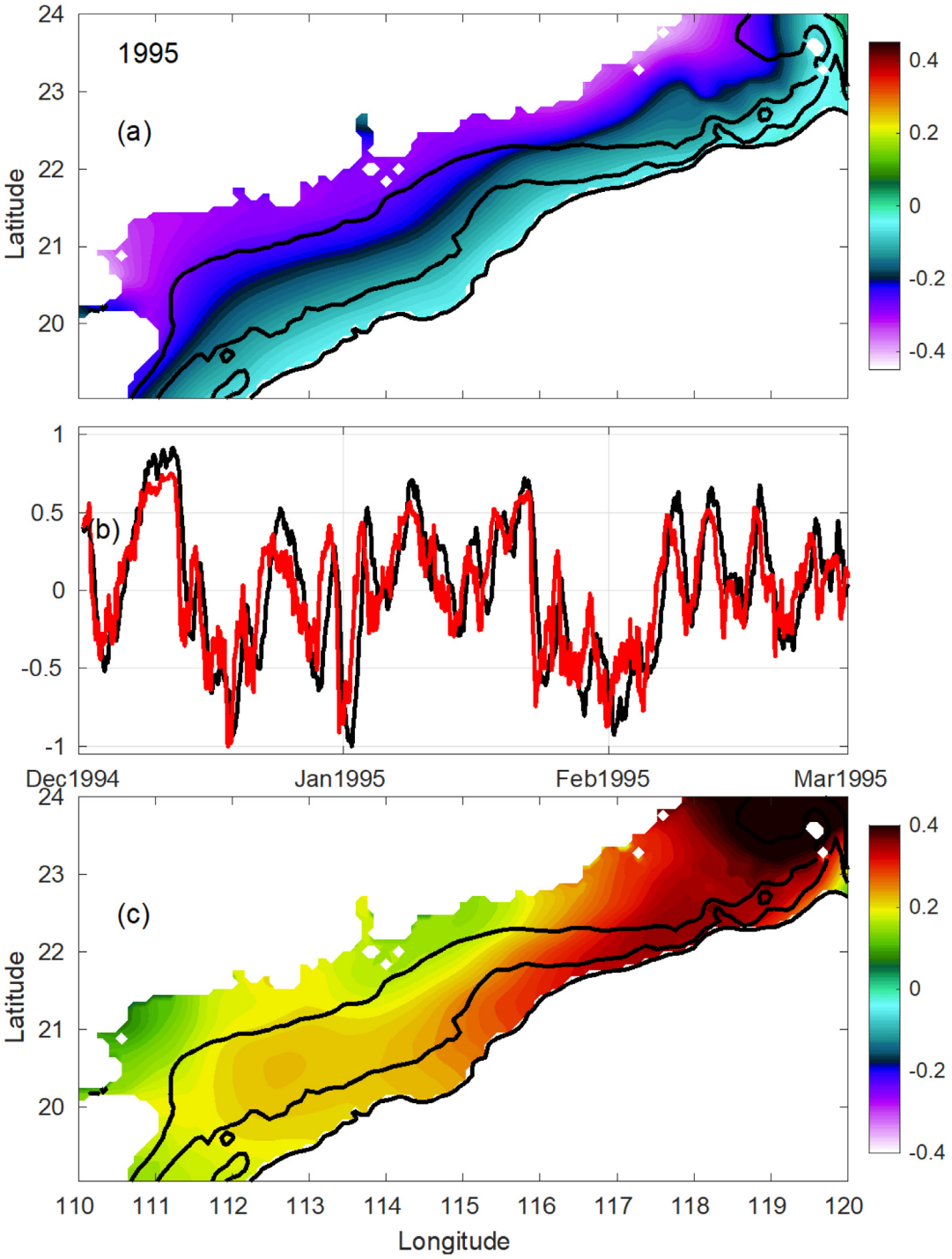

Fig. 3. The spatial pattern of the first SSH EOF mode (a, meters), the normalized expansion coefficient time series (b), and the spatial pattern of the first alongshore wind stress EOF mode (c, N/m^2) from December 1994 to February 1995 from the HYCOM reanalysis. The time series in (b) are normalized by their corresponding magnitude so that these values range from −1 to 1. Black line in (b) represents the SSH time series and red line is for the alongshore wind stress time series. Tick marks in (b) denote the beginnings of the designated months. The EOFs (a, and c) are inflated by the factor of the corresponding magnitude of their time series. The three thick black solid lines in (a) and (c) indicate the 50, 100, and 200 m isobaths, respectively.

points that fall within these boundaries and they all give the same (less than 0.1% difference) results. The green 'x' at 118°E, 22.5°N is one of the 4 grid points that falls within these boundaries (Fig. 1). Thus, this location is chosen as $(i\tau, j\tau)$ where the alongshore wind stress is used to predict the SCSWC and will be referred to as location X hereafter. The sensitivity of the location outside of the common border of all the 90% local variance contours was examined and we found that location X gives the best results for the SCSWC prediction. Results get worse when the location is farther away from the common border of all the 90% local variance contours.

To choose the area for SSH predictions, two more conditions have to be satisfied in addition to the threshold of the 90% local variance explained. Through Ekman dynamics, Yu et al. (2021) demonstrate that the SCSWC originates southwest of Taiwan Strait (their Figure 12 and 8b) instead of near Hainan Island. Thus, the area for SSH predictions should not be in the southwestern part of the domain in Fig. 1. The

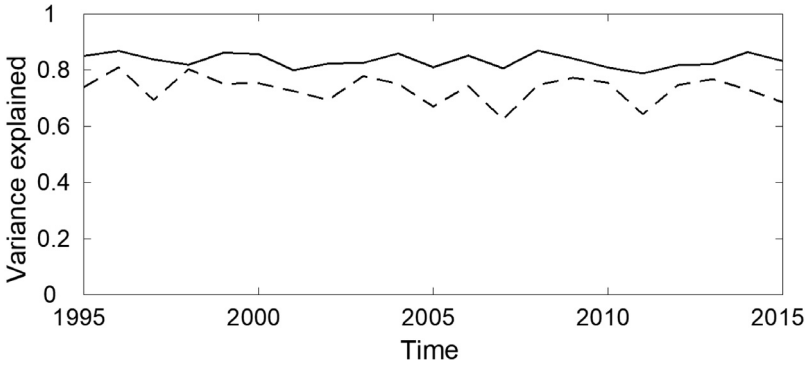

Fig. 4. Total SSH (solid line) and alongshore wind stress (dashed line) variance explained by the leading mode, Ekman transport mode, in each winter (DJF) season.

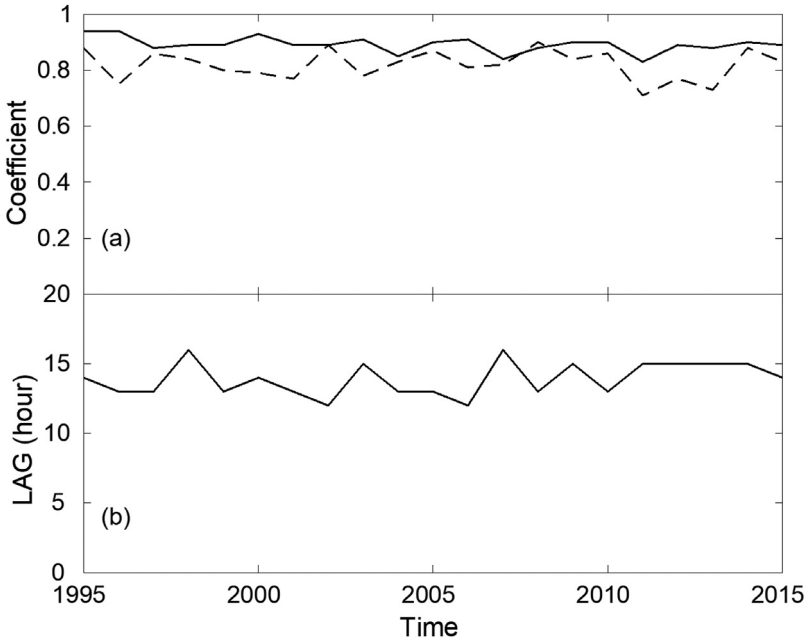

Fig. 5. The maximum lagged correlation coefficient (solid line) of the mode 1 SSH and alongshore wind stress principle component time series and the regression coefficient of the mode 1 SSH principle component time series against the mode 1 alongshore wind stress principle component time series (dashed) (a), and the time lag (hours) associated with the maximum lagged correlation coefficient of the mode 1 SSH and alongshore wind stress principle component time series (b) in each winter (DJF) season.

second condition is that this area needs to be away from the coast since the SCSWC is positioned between the nearshore southwestward Guangdong Coastal Currents and the southward currents along the shelf break that are related to the wind-driven cyclonic gyre in the SCS (Qiu et al., 1985; Guan, 1993); Figures 12c and d in (Yu et al., 2021), i.e. the SCS Branch of the Kuroshio. For these reasons, we choose a 0.8° x 0.5° rectangular area from 115.0° to 116.3°E and 22.1° to 22.6°N (Fig. 1, blue box) (hereafter referred to as the rectangular box) for SSH predictions and thus the SCSWC detection.

3.4. Regression Coefficient of the Mode 1 SSH EOF anomaly against the Mode 1 alongshore wind stress anomaly

The *LRC* in Eq. (7) is a constant for any individual winter season but varies every winter season (Fig. 5a, dashed line). The ratio $\frac{SSH\_EOF1(i,j)}{\tau\_EOF1(i\tau,j\tau)}$ in Eq. (7) is also a constant at any location (i,j) in the rectangular box in each of the 21 winter seasons and also varies every winter season. Thus, $RC(i,j)$ varies every winter season. If the standard deviation of $RC(i,j)$ is much smaller than its 21-year mean, we replace $RC(i,j)$ with its mean and make it interannually independent.

The mean values of $RC(i,j)$ in the 21 winter seasons of the HYCOM reanalysis in the rectangular box (a 6 x 10 matrix) are calculated and shown in Table 1. They are always negative as SSH decreases over the continental shelf when alongshore winds relax, i.e. positive alongshore wind anomaly. Table 1 shows that SSH in the rectangular box (Fig. 1) decreases from −0.45 m at the deeper southeast corner to −0.86 m at the shallower northwest corner after the alongshore wind stress relaxes by 1 N/m^{2}at location X. The standard deviation of $RC(i,j)$ is listed in Table 2 as a ratio to the corresponding 21-season mean. Since the variation is within 8% of the mean, $RC(i,j)$ can be considered to have no interannual dependency to the leading order and we replace $RC(i,j)$ in Eq. (7) with its mean value given in Table 1.

3.5. SCSWC prediction

In Section 3.4, we demonstrate that $RC(i,j)$ is treated as a constant over the 21 winter seasons. Thus, Eq. (6) simply states that mode 1 SSH anomaly ($SSHa1(i,j,t)$) in the rectangular box (Fig. 1) varies linearly with mode 1 alongshore wind stress anomaly at location X, LAG hours earlier ($\tau a1(i\tau,j\tau,t-LAG)$). And in Section 3.3, the SSH (alongshore wind stress) variation in the rectangular box (at the location X) in Fig. 1 can be treated purely as the mode 1 anomaly. But the monthly mean is still needed to calculate the anomaly. To predict the SCSWC from an operational forecast system, neither the monthly mean SSH nor the

Table 1
The mean regression coefficient of mode 1 SSH EOF anomaly on the mode 1 alongshore wind stress anomaly in the 21 winter seasons of the HYCOM reanalysis in the rectangular box as shown in Fig. 1.

Longitude	Latitude									
	115.52	115.6	115.68	115.76	115.84	115.92	116.00	116.08	116.16	116.24
22.56	−.8586	−.8596	−.8552	−.8483	−.8409	−.8335	−.8259	−.8180	−.8081	−.7942
22.48	−.8183	−.8113	−.8019	−.7915	−.7807	−.7705	−.7597	−.7489	−.7374	−.7230
22.40	−.7668	−.7452	−.7405	−.7269	−.7134	−.7010	−.6881	−.6757	−.6636	−.6501
22.32	−.7097	−.6925	−.6752	−.6587	−.6435	−.6302	−.6174	−.6049	−.5928	−.5800
22.24	−.6523	−.6321	−.6119	−.5939	−.5778	−.5644	−.5519	−.5395	−.5269	−.5144
22.16	−.5998	−.5784	−.5570	−.5374	−.5204	−.5054	−.4922	−.4794	−.4664	−.4537

Table 2
The percentage of the standard deviation to the mean regression coefficient of mode 1 SSH EOF anomaly against the mode 1 alongshore wind stress anomaly in the 21 winter seasons of the HYCOM reanalysis in the rectangular box as shown in Fig. 1.

Longitude	Latitude									
	115.52	115.60	115.68	115.76	115.84	115.92	116.00	116.08	116.16	116.24
22.56	7.97	7.91	7.86	7.83	7.81	7.80	7.78	7.75	7.72	7.69
22.48	7.66	7.63	7.63	7.62	7.63	7.63	7.63	7.62	7.61	7.59
22.40	7.45	7.46	7.49	7.49	7.51	7.52	7.55	7.57	7.58	7.58
22.32	7.27	7.31	7.37	7.42	7.48	7.52	7.58	7.67	7.73	7.78
22.24	7.16	7.22	7.32	7.42	7.53	7.62	7.75	7.90	8.05	8.19
22.16	7.22	7.29	7.40	7.52	7.69	7.86	8.05	8.29	8.53	8.77

Table 3
The mean intercept of monthly mean SSH on the monthly mean alongshore wind stress in the 21 winter seasons of the HYCOM reanalysis in the rectangular box as shown in Fig. 1.

Longitude	Latitude									
	115.52	115.6	115.68	115.76	115.84	115.92	116.00	116.08	116.16	116.24
22.56	0.5084	0.5060	0.5039	0.5023	0.5008	0.4992	0.4977	0.4961	0.4950	0.4944
22.48	0.5109	0.5096	0.5087	0.5081	0.5076	0.5070	0.5065	0.5058	0.5055	0.5056
22.40	0.5147	0.5148	0.5153	0.5157	0.5162	0.5165	0.5168	0.5169	0.5172	0.5176
22.32	0.5198	0.5211	0.5226	0.5241	0.5254	0.5264	0.5272	0.5278	0.5284	0.5292
22.24	0.5254	0.5276	0.5300	0.5324	0.5343	0.5357	0.5368	0.5378	0.5388	0.5397
22.16	0.5310	0.5338	0.5368	0.5397	0.5422	0.5442	0.5456	0.5469	0.5482	0.5495

alongshore wind stress are known. Below we show how to use the $RC(i,j)$ in the rectangular box to predict SSH from the alongshore wind stress at location X.

For each winter season, the SSH or wind stress anomaly, is defined as the departure to the monthly mean value are shown below

$$SSHa = SSH - \overline{SSH}, \tag{8a}$$

$$\tau a = \tau - \overline{\tau}, \tag{8b}$$

where, the overbar represents the monthly mean. Rewriting Eq. (6) by replacing the mode 1 anomalies with Eqs. (8a) and (8b), we obtain

$$SSH(i,j,t) - \overline{SSH(i,j)} = RC(i,j) \times \left[\tau(i\tau, j\tau, t - LAG) - \overline{\tau(i\tau, j\tau)}\right]. \tag{9}$$

Rearranging Eq. (9) gives

$$SSH(i,j,t) = RC(i,j) \times \tau(i\tau, j\tau, t - LAG) + Int(i,j), \tag{10}$$

where, the intercept $Int(i,j)$ is defined as

$$Int(i,j) = \overline{SSH(i,j)} - RC(i,j) \times \overline{\tau(i\tau, j\tau)}. \tag{11}$$

For each month of the 21 winter seasons, $Int(i,j)$ is calculated with its corresponding $RC(i,j)$, monthly mean SSH in the rectangular box, and the monthly mean alongshore wind stress at location X. The 21-year mean of $Int(i,j)$ is listed in Table 3 and the corresponding standard deviation is listed in Table 4 as a ratio to the corresponding mean value. The standard deviation is less than 7% of the mean value. So, $Int(i,j)$ has no interannual dependency to the leading order either. Thus, Eq. (10) can be used to predict SSH in the rectangular box from alongshore wind stress at location X using values in Tables 1 and 3.

4. Results

Eq. (10) is applied to both the 21-year HYCOM reanalysis and the GOFS 3.1 7.5-day forecasts to predict SSH in the rectangular box. *LAG* varies from 12 to 16 h and both thresholds mentioned in Section 1 are calculated. The first threshold, area-average negative cross-shore pressure gradient force, gives much better results than the second one. Because the cross-shore velocities are smaller than the alongshore velocities, the non-linear terms in the alongshore direction are bigger than those in the cross-shore direction. This makes the linear dynamics more robust in cross-shore direction than the alongshore direction. We speculate this is why the cross-shore threshold gives better results than the alongshore threshold. In addition, the alongshore threshold also requires additional wind stress information in the rectangular box (Fig. 1). Thus, the negative cross-shore pressure gradient force is a much better SCSWC predictor and the results are limited to this.

4.1. Critical wind stress at location X

From Eq. (10), we can calculate the critical wind stress at location X. The critical wind stress is defined as the wind stress at location X when the area-average cross-shore pressure gradient force by its induced SSH (Eq. (10)) equals to 0. From Eq. (10), this requires

$$MCSG(RC) \times \tau(i\tau, j\tau, t - LAG) + MCSG(Int) = 0, \tag{12}$$

where, *MCSG* denotes the mean cross-shore gradient. The critical alongshore wind stress at location X calculated from Tables 1 and 3 is -0.117 N/m^2 while the 21-winter season mean alongshore wind stress at location X is -0.233 N/m^2. The critical value is 50.2% of the mean wind stress at location X. Thus, the SCSWC occurs in the rectangular box *LAG* hours later if the wind stress at location X relaxes more than 49.8% of its mean value. The SCSWC can also be predicted to the south of the rectangular area when wind relaxes more than the critical value since the SCSWC extends southwestwards as in Yu et al. (2021) and is shown below.

Table 4
The percentage of the standard deviation to the mean intercept in the 21 winter seasons of the HYCOM reanalysis in the rectangular box as shown in Fig. 1.

Longitude	Latitude									
	115.52	115.60	115.68	115.76	115.84	115.92	116.00	116.08	116.16	116.24
22.56	6.79	6.79	6.79	6.77	6.75	6.73	6.70	6.68	6.65	6.60
22.48	6.66	6.64	6.61	6.58	6.55	6.51	6.48	6.44	6.41	6.36
22.40	6.50	6.48	6.45	6.42	6.39	6.36	6.33	6.30	6.27	6.23
22.32	6.36	6.36	6.35	6.33	6.31	6.28	6.26	6.24	6.22	6.19
22.24	6.29	6.30	6.29	6.29	6.28	6.27	6.26	6.25	6.23	6.22
22.16	6.29	6.30	6.29	6.29	6.29	6.29	6.29	6.29	6.28	6.27

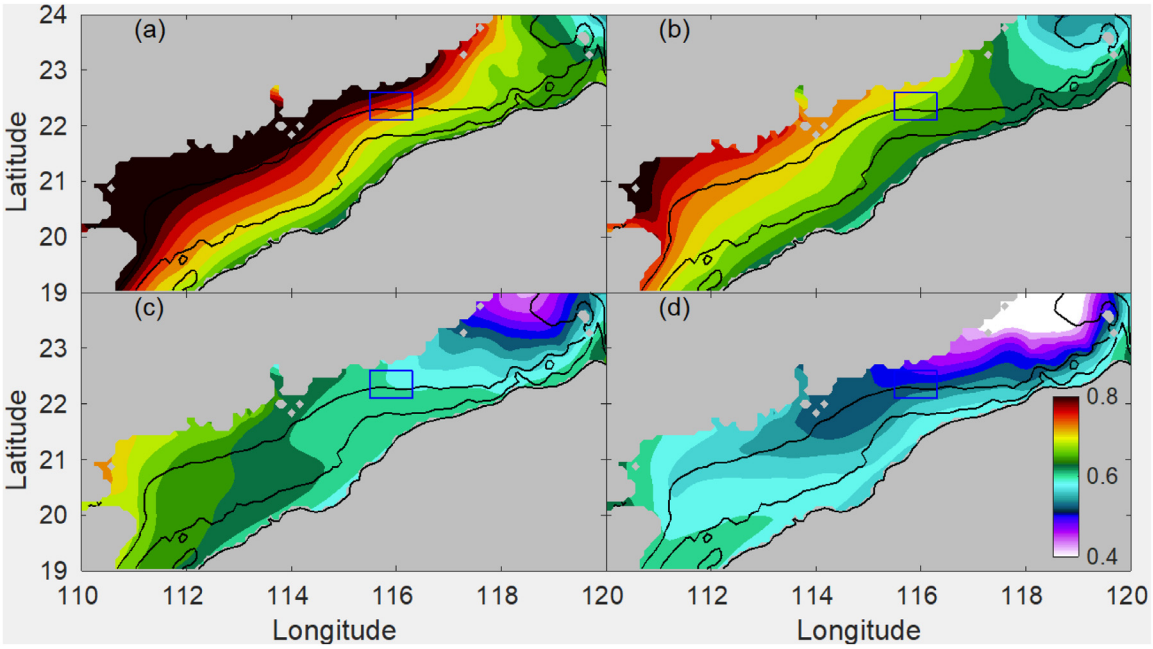

Fig. 6. Sea surface height (m) predicted from Eq. (10) using *RC* and *Int* over the whole shelf for the following cases: wind burst (a, $\tau = -0.350$ N/m^2), mean wind (b, $\tau = -0.233$ N/m^2), critical wind stress (c, $\tau = -0.117$ N/m^2), and zero alongshore wind stress (d) at location X (Fig. 1).

SSH over the whole continental shelf is predicted with Eq. (10) using *RC* and *Int* over the whole shelf (not shown) and are shown in Fig. 6 for the following cases: wind burst (Fig. 6a, $\tau = -0.350$ N/m^2), mean wind (Fig. 6b, $\tau = -0.233$ N/m^2), critical wind stress (Fig. 6c, $\tau = -0.117$ N/m^2), and zero alongshore wind stress (Fig. 6d). The wind burst case is defined as the alongshore wind stress at location X that is 50% stronger than the 21-winter season mean. SSH from the reanalysis that are 14 h after the alongshore wind stress at location X that correspond to the four cases are shown in Figures 7a (wind burst), 7b (mean wind), 7c (critical wind stress) and 7d (zero alongshore wind stress). Fig. 6a indicates that the southwestward geostrophic currents associated with the predicted SSH during a wind burst are stronger than those from the mean wind stress (Fig. 6b). There are weak negative (positive) alongshore geostrophic currents in the northwest (southeast) portion of the rectangular box (Fig. 6c) from the predicted SSH using critical wind stress, but the area-average alongshore geostrophic current is zero in the box. When wind further relaxes, there are positive alongshore geostrophic currents everywhere in the rectangular box and most of the shelf to the south of the box (Fig. 6d). All of these are in good agreement with the reanalysis (Fig. 7).

4.2. Performance of the method

The prediction is compared with the HYCOM outputs. The occurrence of the SCSWC is defined as a positive mean HYCOM alongshore barotropic velocity in the rectangular box. Two criteria define the performance of the method. The first shows the accuracy, which is defined as the ratio that the prediction is consistent with the occurrence of the SCSWC. The second criterion shows the representativeness, defined as how many of the total occurrences of the SCSWC are represented by the prediction. The method accuracy and representativeness are given in Table 5 for all predictions using Eq. (10) or the -0.117 N/m^2 critical alongshore wind stress at location X with time lags vary from 12 to 16 h.

When predicting the SCSWC using the wind stress from the 4 years of GOFS 3.1 7.5-day forecasts at the location X, the mean accuracy of this method varies from 69.2% to 69.7% (Table 5) with different *LAG*. The mean representativeness varies from 86.2% to 88.0% with different *LAG*.

When applying the method to predict the SCSWC for the 21-winters on wind stress data from the HYCOM reanalysis, the mean accuracy varies from 74.9% to 75.3% (Table 5) during the 21-winter seasons with difference *LAG*, which is slightly higher than those from the operational GOFS 3.1 forecasts. But the mean representativeness is slightly lower and varies from 84.5% to 85.9% with different *LAG* during the 21-winter seasons. This difference will be discussed in Section 5.1.

In both the HYCOM reanalysis and GOFS 3.1 forecasts, the time lag (*LAG*) does not make a big difference to the performance. So, any of the 5 time lags, from 12 to 16 h, can be used to predict the SCSWC depending on the temporal frequency of the wind stress data.

5. Conclusions and discussions

In this study, we developed an empirical method to predict the counter-wind SCSWC in the rectangular area using wind stress at

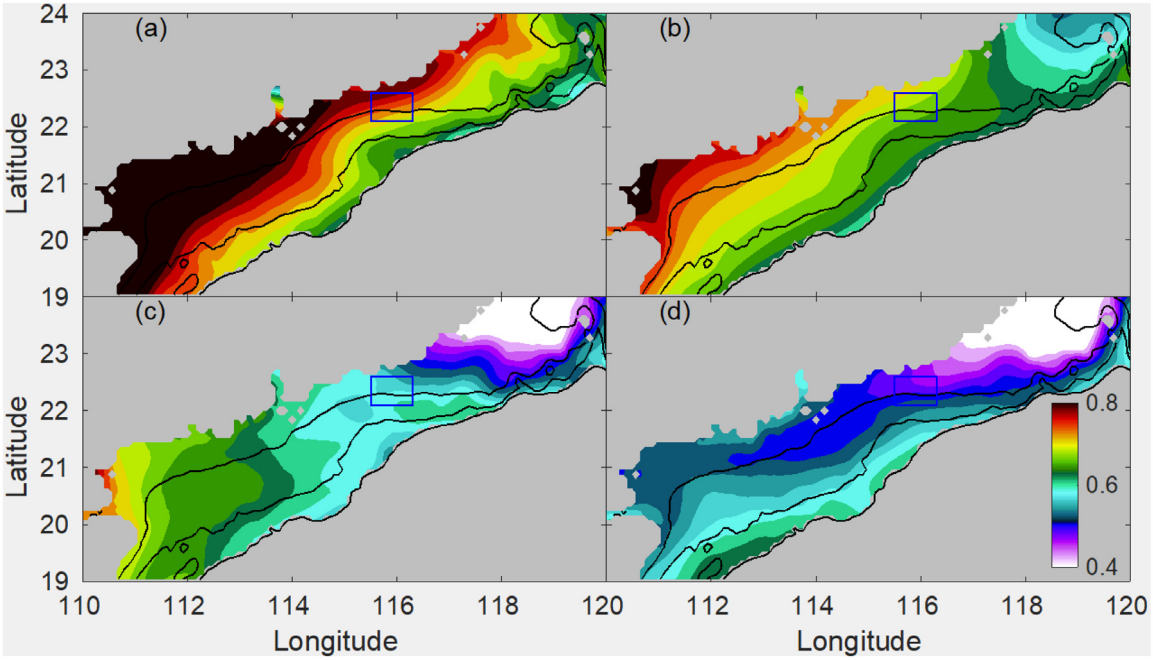

Fig. 7. Reanalysis sea surface height (m) 14 h after the alongshore wind stress at location X (Fig. 1) equals the value used to represent the following cases: wind burst (a, $\tau = -0.350$ N/m^2), mean wind (b, $\tau = -0.233$ N/m^2), critical wind stress (c, $\tau = -0.117$ N/m^2), and zero alongshore wind stress (d).

Table 5
The performance of Eq. (10) on GOFS 3.1 forecasts and the HYCOM reanalysis.

	LAG	12	13	14	15	16
GOFS 3.1 Forecasts	Accuracy	69.2%	69.5%	69.7%	69.7%	69.6%
	Representativeness	88.0%	87.7%	87.4%	86.8%	86.2%
HYCOM Reanalysis	Accuracy	75.1%	75.3%	75.3%	75.2%	74.9%
	Representativeness	84.8%	85.0%	85.0%	85.9%	84.5%

location X. The method is built on the Ekman mode, the most dominant EOF mode of the SSH over the SCS continental shelf. The method predicts SSH from the alongshore wind stress at location X. When the area-average cross-shore pressure gradient force in the rectangular area is negative, the method predicts the occurrence of the SCSWC in the rectangular area. The critical alongshore wind stress at location X is calculated as -0.117 N/m^2.

Applying the method to the HYCOM reanalysis shows accuracy of 75.3% and representativeness of 85.3% with 14-hour time lag. For the 4 years of GOFS 3.1 7.5-day forecasts, the method shows a 69.7% accuracy and 87.4% representativeness with the same time lag.

5.1. Why the method has better accuracy and worse representativeness on HYCOM reanalysis than the GOFS 3.1 forecasts

One might expect to have better accuracy when applying the method to the HYCOM reanalysis since the method is derived from it. But why does the method shows a lower representativeness on HYCOM reanalysis than GOFS 3.1 forecasts? The reason is the different time frame.

The HYCOM reanalysis covers 21 winter seasons from 1995 to 2015 while the GOFS 3.1 forecasts are for 4 winter seasons from 2018 to 2021. The mean representativeness of each individual winter season from the HYCOM reanalysis with 14-hour *LAG* actually varies from 68.1% (1997) to 97.8% (2013). Since the GOFS 3.1 forecasts are outside the reanalysis time frame, it is possible that these 4-winter seasons have higher representativeness.

The different time frame also affects the calculation of *Int* in Eq. (10). Please note that the $RC(i,j)$ in Eq. (10) represents the dynamics of the most dominant SSH mode (the Ekman mode), which is independent of the source of the wind forcing, over the continental shelf of the SCS. But *Int* is monthly mean *SSH* and τ dependent according to Eq. (11). Thus, *Int* depends on the source of the wind forcing, CFSR (HYCOM reanalysis) vs NAVGEM (GOFS 3.1 reanalysis) and time duration. The 4-winter season mean alongshore wind stress in GOFS 3.1 forecasts at location X is -0.203 N/m^2, which is 87% of the HYCOM reanalysis mean. The critical alongshore wind stress, -0.117 N/m^2, represents a 42.4% wind relaxation instead of 49.8% as in HYCOM reanalysis. This implies a looser threshold to detect SCSWC in GOFS 3.1 forecasts, which means the method captures more SCSWC events in GOFS 3.1 forecasts (more representativeness) but also more false predictions (less accuracy).

5.2. Positive alongshore wind stress in the rectangular box

The positive mean alongshore wind stress represents a special case of the alongshore dynamics. It happens when the wind relaxes so much that it actually reverses its direction from southwestward to northeastward, in the same direction with the SCSWC. Yu et al. (2021) have shown that the wind relaxation enhances the positive alongshore pressure gradient force (their Fig. 7b). Thus, the positive alongshore wind stress automatically satisfies the alongshore SCSWC dynamics threshold. So, when the mean wind stress in the rectangular box is positive (northeastward), we predict there is SCSWC. For the 21 winter seasons in reanalysis and the 4 winter seasons in the GOFS 3.1 7.5-day forecasts, positive mean alongshore wind stress in the rectangular box occurs just about 2% of the time. And the accuracy of the predicted SCSWC occurrence in both products is about 96%. So the SCSWC is almost guaranteed to occur when the mean alongshore wind stress is positive in the rectangular box (Fig. 1). The dynamics behind this is that both alongshore pressure gradient force and wind stress are positive, which requires negative friction (positive alongshore currents,

the SCSWC) and Coriolis force (cross-shore outflow) to balance the force.

5.3. Linear regression of SSH on alongshore wind stress

The method introduced above is similar to calculating the regression coefficient and intercept of SSH in the rectangular box against the alongshore wind stress at location X, but they are slightly different. The difference mainly comes from the time lag. At each winter season, the time lag associated with the maximum correlation coefficient between SSH at each location in the rectangular box and wind stress at location X is space dependent instead of a constant value as in EOF analysis. These time lags vary from 4 h to 14 h in the rectangular box. If we use the space dependent time lag to calculate the regression coefficients and intercepts, the SCSWC prediction accuracy is ~3.2% less than the results shown in Section 4.1 but the representativeness is almost the same.

5.4. Sources of prediction error

As mentioned above, this method is easy to use and performs reasonably well. But there are different sources of errors. Below we discuss where the errors mainly come from.

We first discuss the dynamics. The empirical method is built on the linear dynamics revealed by Yu et al. (2021). The cross-shore dynamics threshold is the negative mean cross-shore pressure gradient force in the rectangular box so that the mean alongshore geostrophic current is northeastward. This assumes steady state and totally ignores the horizontal advection (nonlinearity). In reality, the cross-shore pressure gradient can also be balanced by the time tendency of the alongshore currents and horizontal advection. Over the 21-winter seasons of the HYCOM reanalysis, 1.1% of the mean positive alongshore barotropic velocity in the rectangular box are associated with positive cross-shore pressure gradient force. And when the mean cross-shore pressure gradient force is negative in the rectangular box, 29.7% of the time the mean alongshore barotropic currents in the box are negative. By our definition, this represents 70.3% of accuracy and 98.9% of representativeness.

The second source of errors comes from building the method on Ekman dynamics, which is the leading mode of the SSH EOFs. There are other dynamical modes that explain up to 10% of the SSH variations in the rectangular box. If we reconstruct the SSH field with the leading SSH mode and apply the dynamic threshold to the rectangular box, the corresponding accuracy is 76.2% and the representativeness is 88.3%. These two numbers represent the ceiling of the empirical method.

Thirdly, we ignore the variation of the regression coefficient and intercept based on a less than 10% standard deviation (Sections 3.4 and 3.5). We use the mean values so that Eq. (10) can be applied to any given winter season and provide the best overall prediction. But doing so also generates error. Comparing the performance of the method over the HYCOM reanalysis (Table 5) with the ceilings of this method (last paragraph), we lose 1.0% of the accuracy and 4.0% of the representativeness.

Declaration of competing interest

The authors declare that they have no known competing financial interests or personal relationships that could have appeared to influence the work reported in this paper.

Acknowledgments

The authors thank the editor and three anonymous reviewers for their input to improve the original manuscript. Financial support for Z. Yu and E. J. Metzger is provided by the “6.1 South China Sea Dynamics” project sponsored by the Office of Naval Research under program element 0601153N. Y. Fan is funded by the “6.2 Turbulent Mixing in NCOM and HYCOM” project sponsored by the Office of Naval Research under program element 062435N. Computer time was provided by the Department of Defense (DoD) High Performance Computing Modernization Program and the simulations were performed on the Cray XC40 (Conrad) at the Navy DoD Supercomputing Resources Center, Stennis Space Center, MS. The output used in the research are served at https://www.hycom.org. This is NRL contribution NRL/JA/7320-22-5447. It has been approved for public release and distribution is unlimited.

References

Bleck, R., 2002. An oceanic general circulation model framed in hybrid isopycnic-Cartesian coordinates. Ocean Model. 4, 55–88.

Bloom, S.C., Takacs, L.L., da Silva, A.M., Ledvina, D., 1996. Data assimilation using incremental analysis updates. Mon. Wea. Rev. 124, 1256–1271.

Chao, S.Y., Shaw, P.T., Wang, J., 1995. Wind relaxation as a possible cause of the South China Sea Warm Current. J. Oceanogr. 51 (1), 111–132.

Chiang, T.-L., Wu, C.-R., Chao, S.-Y., 2008. Physical and geographical origins of the South China Sea Warm Current. J. Geophys. Res. 113, C08028. http://dx.doi.org/10.1029/2008JC004794.

Cummings, J.A., Smedstad, O.M., 2014. Ocean data impact in global HYCOM. J. Atmos. Ocean. Technol. 31, 1771–1791. http://dx.doi.org/10.1175/jtech-d-14-00011.1.

Fang, W., Guo, P., Liu, C., Fang, G., Li, S., 2015. Observed sub-inertial current variability and volume transport over the continental shelf in the northern South China Sea. Estuar. Coast. Shelf Sci. 157, 19–31. http://dx.doi.org/10.1016/j.ecss.2015.02.001.

Guan, B.X., 1986. Evidence for a counter-wind current in winter off the southeast coast of China. Chin. J. Oceanol. Limnol. 4 (4), 319–332.

Guan, B.X., 1993. Winter counter-wind current off the southeastern China coast and a preliminary investigation of its source. In: Proceedings of the Symposium on the Physical and Chemical Oceanography of the China Seas. China Ocean Press, Beijing, pp. 1–9.

Guan, B.X., Chen, S.J., 1964. The current systems in the near-sea area of China seas. p. 85 (in Chinese).

Guan, B., Fang, G., 2006. Winter counter-wind currents off the southeastern China coast: A review. J. Oceanogr. 62, 1–24. http://dx.doi.org/10.1007/s10872-006-0028-8.

Hogan, T.F., Liu, M., Ridout, J.A., Peng, M.S., Whitcomb, T.R., Ruston, B.C., Reynolds, C.A., Eckermann, S.D., Moskaitis, J.R., Baker, N.L., McCormack, J.P., Viner, K.C., McLay, J.G., Flatau, M.K., Xu, L., Chen, C., Chang, S.W., 2014. The navy global environmental model. Oceanography 27, 116–125. http://dx.doi.org/10.5670/oceanog.2014.66.

Hsueh, Y., Zhong, L., 2004. A pressure-driven South China Sea Warm Current. J. Geophys. Res. 109, C09014. http://dx.doi.org/10.1029/2004JC002374.

Hu, J.Y., Kawamura, H., Hong, H., Qi, Y.Q., 2000. A review on the currents in the South China Sea: Seasonal circulation, South China Sea Warm Current and Kuroshio intrusion. J. Oceanogr. 56, 607–624.

Li, R.F., Zeng, Q.C., Gan, Z.J., Wang, W.Z., 1993. Numerical simulation of the South China Sea Warm Current and the Taiwan Strait flow in winter. Prog. Nat. Sci. 3 (2), 123–129.

Li, R.F., Zeng, Q.C., Ji, Z.Z., Gun, D., 1992. Numerical simulation for a northeastward flowing current from area off the eastern Hainan Island to Tsugaru/Soya Strait. La Mer 30, 229–238.

Metzger, E.J., Smedstad, O.M., Thoppil, P.G., Hurlburt, H.E., Cummings, J.A., Wallcraft, A.J., Zamudio, L., Franklin, D.S., Posey, P.G., Phelps, M.W., Hogan, P.J., Bub, F.L., Dehaan, C.J., 2014. US navy operational global ocean and arctic ice prediction systems. Oceanography 27, 32–43.

Qiu, D.Z., Huang, Y.T., Chen, L.M., Guo, Z.X., 1985. Circulation structures in the studied waters. In: South China Sea Institute of Oceanology (Ed.), Comprehensive Investigations and Studies of the South China Sea (2). Chinese Academy of Sciences, Science Press, Beijing, pp. 204–230 (in Chinese).

Saha, S., et al., 2010. The NCEP climate forecast system reanalysis. Bull. Am. Meteorol. Soc. 91, 1015–1057. http://dx.doi.org/10.1175/2010BAMS3001.1.

Saha, S., et al., 2014. The NCEP climate forecast system version 2. J. Clim. 27, 2185–2208. http://dx.doi.org/10.1175/JCLI-D-12-00823.1.

Shaw, P.T., Chao, S.Y., 1994. Surface circulation in the South China Sea. Deep-Sea Res. I 40 (11/12), 1663–1683.

Su, J.L., Wang, W., 1987. On the sources of the Taiwan Warm Current from the South China Sea. Chin. J. Oceanol. Limnol. 5 (4), 299–308.

Wang, D., Hong, B., Gan, J., Xu, H., 2010. Numerical investigation on propulsion of the counter-wind current in the northern South China Sea in winter. Deep-Sea Res. I 57, 1206–1221. http://dx.doi.org/10.1016/j.dsr.2010.06.007.

Wyrtki, K., 1961. Physical oceanography of the Southeast Asian water. In: NAGA Report 2, Scientific Result of Marine Investigation of the South China Sea and Gulf of Thailand 1959–1961. Scripps Institution of Oceanography, La Jolla, California, p. 195.

Xue, H., Chai, F., Pettigrew, N., Xu, D., Shi, M., Xu, J., 2004. Kuroshio intrusion and the circulation in the South China Sea. J. Geophys. Res. 109, C02017. http://dx.doi.org/10.1029/2002JC001724.

Yang, J., Wu, D., Lin, X., 2008. On the dynamics of the South China Sea Warm Current. J. Geophys. Res. 113, C08003. http://dx.doi.org/10.1029/2007JC004427.

Ye, L., 1994. On the mechanism of South China Sea warm Current and Kuroshio Branch in winter - Preliminary result of 3-D baroclinic experiments. Terr. Atmos. Oceanic Sci. 5 (4), 597–610.

Yu, Z., Metzger, E.J., Fan, Y., 2017. The impact of ocean surface currents on Sverdrup transport in the midlatitude north Pacific via the wind stress formulation. J. Phys. Oceanogr. 47, http://dx.doi.org/10.1175/JPO-D-16-0155.1.

Yu, Z., Metzger, E.J., Fan, Y., 2021. Generation mechanism of the counter-wind South China Sea Warm Current in winter. Ocean Model. http://dx.doi.org/10.1016/j.ocemod.2021.101875.

Zeng, Q., Li, R., Ji, Z., Gan, Z., Ke, P., 1989. Calculations of the monthly mean circulation in the South China Sea. Sci. Atmos. Sin. 13, 127–168 (in Chinese).

Zhai, L., Fang, G., Wang, K., 2004. Numerical study on the dynamics of wind driven barotropic circulation in the South China Sea. Oceanol. Limnol. Sin. 35 (4), 289–298 (in Chinese with English abstract).

Zhong, H.L., 1990. Structures of the density circulation. In: Ma, Y.L., et al. (Eds.), Report of Decadal Hydrographic Series Survey of the Shelf, Adjacent Waters of the Northern South China Sea. China Ocean Press, Beijing, pp. 215–241 (in Chinese).